Berry Curvature Spectroscopy from Bloch Oscillations

Christophe De Beule[1,2,*] and E. J. Mele[1]
[1]Department of Physics and Astronomy, University of Pennsylvania, Philadelphia, Pennsylvania 19104, USA
[2]Department of Physics and Materials Science, University of Luxembourg, L-1511 Luxembourg, Luxembourg

(Received 23 May 2023; revised 21 August 2023; accepted 10 October 2023; published 9 November 2023)

Artificial crystals such as moiré superlattices can have a real-space periodicity much larger than the underlying atomic scale. This facilitates the presence of Bloch oscillations in the presence of a static electric field. We demonstrate that the optical response of such a system, when dressed with a static field, becomes resonant at the frequencies of Bloch oscillations, which are in the terahertz regime when the lattice constant is of the order of 10 nm. In particular, we show within a semiclassical band-projected theory that resonances in the dressed Hall conductivity are proportional to the lattice Fourier components of the Berry curvature. We illustrate our results with a low-energy model on an effective honeycomb lattice.

DOI: 10.1103/PhysRevLett.131.196603

Nonlinear optical responses are becoming an increasingly important tool to investigate the spectral and geometric properties of electron Bloch bands in low-dimensional materials [1–3]. In particular, the nonlinear Hall effect [4] which probes multipoles of the Berry curvature of the band at successive orders in the driving field [5]. Importantly, since time-reversal symmetry only precludes odd powers of the field in the Hall response, nonlinear responses allow one to study the momentum-space distribution of the Berry curvature even in systems with time-reversal symmetry. Recently, the advent of moiré [6–8] and other two-dimensional (2D) artificial crystals [9–11] has opened up the prospect of studying responses at nonperturbative order in the driving field [12–14]. These systems can host spectrally isolated and flattened minibands, and nonlinear responses have already been used to study their properties [15–22]. Moreover, because the real-space periodicity of these systems can be much larger than the underlying atomic scale periodicity, with lattice constants ranging between 1–100 nm, the momentum space Brillouin zone (BZ) is relatively small. Under an applied electric field, it therefore becomes possible for an electron to traverse the *entire* zone, i.e., perform a full Bloch oscillation [23,24], before relaxing to equilibrium by scattering. To quantify this regime, consider an applied uniform electric field of the form

$$\boldsymbol{E}(t) = \boldsymbol{E}_0 + \boldsymbol{E}_1(t), \tag{1}$$

which has a static component $\boldsymbol{E}_0 = E_0(\cos\theta_0, \sin\theta_0)$ and an oscillating component $\boldsymbol{E}_1(t)$. The latter acts as a weak probe for the system that is *dressed* by the static field. Here, the nonperturbative regime is defined by the condition $\omega_B\tau \gg 1$ [12–14] where $\omega_B = eE_0L/\hbar$ is the Bloch frequency, i.e., the characteristic frequency of Bloch oscillations, and τ is the momentum-relaxation time with L the lattice constant. If we estimate $\tau = 1$ ps we find that $\omega_B\tau \approx [1.5E_0/(\mathrm{kV/cm})][L/(10\ \mathrm{nm})]$ such that $\omega_B\tau$ can become large in artificial crystals for reasonable field strengths [12,13].

In this work, we study the dressed time-dependent response of time-reversal-invariant 2D artificial lattices with lattice constants $L \sim 10$ nm, that are subjected to a uniform electric field of the form given in Eq. (1). This setup is illustrated in Fig. 1(a). When the static field is in the

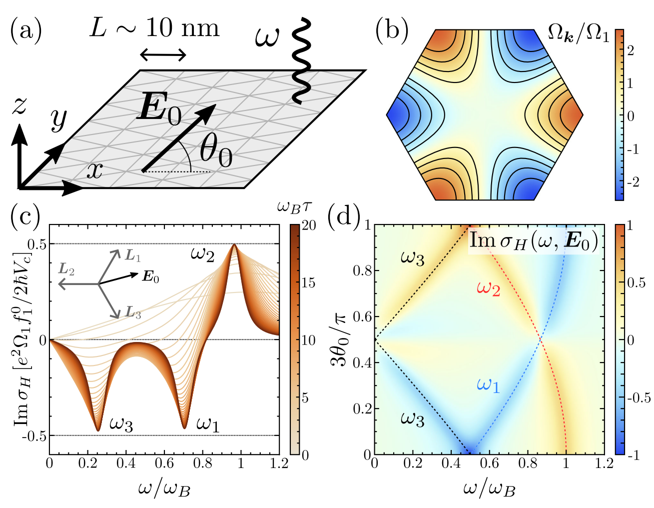

FIG. 1. (a) A 2D artificial crystal (e.g., a moiré) subjected to a static uniform in-plane electric field $\boldsymbol{E}_0$ and probed by monochromatic light of frequency ω. (b) Berry curvature $\Omega_{\boldsymbol{k}}$ in the first-shell approximation for a system with D_3 or C_{3v} symmetry. (c) Imaginary part of the dressed optical Hall conductivity $\sigma_H(\omega, \boldsymbol{E}_0)$ for the Berry curvature shown in (b) as a function of ω/ω_B for $\theta_0 = 15°$ and different values of $\omega_B\tau$. (d) $\mathrm{Im}\sigma_H$ in units $e^2\Omega_1 f_1^0/2\hbar V_c$ for $\omega_B\tau = 15$ as a function of the frequency and the field direction θ_0. The resonant frequencies for the first shell $\omega_n = |e\boldsymbol{E}_0 \cdot \boldsymbol{L}_n/\hbar|$ are indicated.

regime of Bloch oscillations, we find an optical response, linear in the *oscillating* component, that is resonant at the Bloch frequencies. For the studied systems, the latter are on the order of 5–10 THz. Moreover, we show that the peak heights of the resonances in the dressed optical *Hall* conductivity are proportional to the Fourier components of the Berry curvature. Hence, our approach is in some sense dual to probing the momentum-space distribution of the Berry curvature via its multipoles at successive harmonics [25] and complementary to other methods, e.g., measuring orbital moments with circular dichroism [26]. In contrast, in our proposal, all information on the Berry curvature is contained in the dressed *linear* optical response and contributions from different Fourier components can be favored by varying the direction of the static field.

Semiclassical theory.—Our starting point is the band-projected semiclassical theory of electron dynamics for a 2D crystal in a uniform electric field $\boldsymbol{E}(t)$. The equations of motion for the central position and crystal momentum of a wave packet constructed from the Bloch states of an energy band $\varepsilon_{n\boldsymbol{k}}$ are given by [27,28]

$$\hbar\dot{\boldsymbol{r}}_{n\boldsymbol{k}} = \nabla_{\boldsymbol{k}}\varepsilon_{n\boldsymbol{k}} - \hbar\dot{\boldsymbol{k}} \times \Omega_{n\boldsymbol{k}}\hat{z}, \tag{2}$$

$$\hbar\dot{\boldsymbol{k}} = -e\boldsymbol{E}(t), \tag{3}$$

where $-e$ is the electron charge and $\Omega_{n\boldsymbol{k}} = -2\mathrm{Im}\langle\partial_{k_x}u_{n\boldsymbol{k}}|\partial_{k_y}u_{n\boldsymbol{k}}\rangle_{\mathrm{cell}}$ is the Berry curvature [29]. The band-projected theory holds as long as interband transitions can be neglected. These can arise both from optical transitions and electric breakdown (Zener tunneling) [31]. The former are absent for frequencies below the energy gap to the other energy bands $\varepsilon_{\mathrm{gap}}$, while the absence of the latter can be estimated by the condition that $\varepsilon_{\mathrm{gap}}^2/\varepsilon_{\mathrm{width}} \gg eE_0L$ where $\varepsilon_{\mathrm{width}}$ is the bandwidth. Hence, we consider the intermediate regime $\hbar/\tau \ll eE_0L \ll \varepsilon_{\mathrm{gap}}^2/\varepsilon_{\mathrm{width}}$ [12–14].

In the following, we drop the band index n since we consider a single band. The current is then given by

$$\boldsymbol{j}(t) = -e\int_{\boldsymbol{k}} \dot{\boldsymbol{r}}_{\boldsymbol{k}}(t)f_{\boldsymbol{k}}(t), \tag{4}$$

with $\int_{\boldsymbol{k}} = \int_{\mathrm{BZ}} d^2\boldsymbol{k}/(2\pi)^2$ and where $f_{\boldsymbol{k}}(t)$ is the nonequilibrium occupation of the electrons in the band. The latter is obtained from the Boltzmann transport equation in the relaxation-time approximation:

$$\tau\partial_t f_{\boldsymbol{k}} - \frac{e\tau}{\hbar}\boldsymbol{E}(t)\cdot\nabla_{\boldsymbol{k}} f_{\boldsymbol{k}} = f_{\boldsymbol{k}}^0 - f_{\boldsymbol{k}}, \tag{5}$$

where τ is the momentum-relaxation time and $f_{\boldsymbol{k}}^0 = n_F(\varepsilon_{\boldsymbol{k}} - \mu)$ with n_F the Fermi function and μ the chemical potential. Because the system has translational symmetry, the occupation function is periodic in momentum space: $f_{\boldsymbol{k}} = \sum_{\boldsymbol{R}} f_{\boldsymbol{R}} e^{i\boldsymbol{k}\cdot\boldsymbol{R}}$ where the sum runs over lattice vectors $\boldsymbol{R}$ with $f_{\boldsymbol{R}} = V_c\int_{\boldsymbol{k}} f_{\boldsymbol{k}} e^{-i\boldsymbol{k}\cdot\boldsymbol{R}}$. Plugging this expansion in Eq. (5) we obtain an ordinary differential equation with the steady-state solution [32]

$$f_{\boldsymbol{R}}(t) = f_{\boldsymbol{R}}^0 \int_0^\infty ds\, e^{-s} \exp\left[\frac{ie}{\hbar}\int_{t-s\tau}^{t} dt'\, \boldsymbol{E}(t')\cdot\boldsymbol{R}\right], \tag{6}$$

as shown in Supplemental Material (SM) [33]. The occupation $f_{\boldsymbol{k}}$ is thus given by a weighted sum of displaced Fermi functions where the drift due to the electric field is determined by the accumulated momentum between collisions at time $t - s\tau$ and time t. Here, the exponential weight e^{-s} reflects the fact that scattering is modeled as a Poisson process.

The current in Eq. (4) can be decomposed into two terms as $\boldsymbol{j}(t) = \boldsymbol{j}_{\mathrm{Bloch}}(t) + \boldsymbol{j}_{\mathrm{geom}}(t)$ where

$$\boldsymbol{j}_{\mathrm{Bloch}}(t) = \frac{ie}{\hbar V_c}\sum_{\boldsymbol{R}} \boldsymbol{R}\varepsilon_{-\boldsymbol{R}} f_{\boldsymbol{R}}(t), \tag{7}$$

$$\boldsymbol{j}_{\mathrm{geom}}(t) = \hat{z}\times\frac{e^2}{\hbar V_c}\sum_{\boldsymbol{R}} \Omega_{-\boldsymbol{R}}\boldsymbol{E}(t) f_{\boldsymbol{R}}(t), \tag{8}$$

where V_c is the unit cell area and we made use of the expansions of the band dispersion and the Berry curvature, as well as $V_c\int_{\boldsymbol{k}} e^{i\boldsymbol{k}\cdot\boldsymbol{R}} = \delta_{\boldsymbol{R},\boldsymbol{0}}$. The Bloch current $\boldsymbol{j}_{\mathrm{Bloch}}$ originates from the band dispersion while the geometric current $\boldsymbol{j}_{\mathrm{geom}}$ originates from the anomalous velocity due to the Berry curvature in Eq. (2).

Dressed optical conductivity.—We now consider probing the system with monochromatic light of frequency ω that is incident normal to the xy plane. In the electric-dipole approximation, the electric field of the light can be written as

$$\boldsymbol{E}_1(t) = \boldsymbol{\mathcal{E}}_1 e^{i\omega t} + \boldsymbol{\mathcal{E}}_1^* e^{-i\omega t}, \tag{9}$$

where $\boldsymbol{\mathcal{E}}_1 \in \mathbb{C}^2$ gives the amplitude and polarization. To investigate the response at frequency ω, we expand each lattice Fourier component of the distribution function in its frequency components. We have $f_{\boldsymbol{R}}(t) = \sum_{m=-\infty}^{\infty} f_{\boldsymbol{R},m} e^{im\omega t}$ where $f_{\boldsymbol{R},m} = (\omega/2\pi)\int_0^{2\pi/\omega} dt f_{\boldsymbol{R}}(t)e^{-im\omega t}$ with $f_{\boldsymbol{R},-m} = f_{-\boldsymbol{R},m}^*$. The frequency components of the currents become

$$\boldsymbol{j}_{\mathrm{Bloch}}^{(m)} = \frac{ie}{\hbar V_c}\sum_{\boldsymbol{R}} \boldsymbol{R}\varepsilon_{-\boldsymbol{R}} f_{\boldsymbol{R},m}, \tag{10}$$

$$\boldsymbol{j}_{\mathrm{geom}}^{(m)} = \hat{z}\times\frac{e^2}{\hbar V_c}\sum_{\boldsymbol{R}} \Omega_{-\boldsymbol{R}}(\boldsymbol{E}_0 f_{\boldsymbol{R},m} + \boldsymbol{\mathcal{E}}_1 f_{\boldsymbol{R},m-1} + \boldsymbol{\mathcal{E}}_1^* f_{\boldsymbol{R},m+1}). \tag{11}$$

Since we are interested in the linear response *dressed* by the static part of the field, we expand Eq. (6) in orders of

$e\boldsymbol{\mathcal{E}}_1 \cdot \boldsymbol{R}/\hbar\omega$ while retaining all orders in $\boldsymbol{E}_0$. Up to first order, the only nonzero terms are given by

$$f_{\boldsymbol{R},0} = \frac{f^0_{\boldsymbol{R}}}{1 - i\omega_{\boldsymbol{R}}\tau}, \tag{12}$$

$$f_{\boldsymbol{R},1} = \frac{f^0_{\boldsymbol{R}}}{1 - i\omega_{\boldsymbol{R}}\tau} \frac{e\boldsymbol{\mathcal{E}}_1 \cdot \boldsymbol{R}/\hbar}{\omega - \omega_{\boldsymbol{R}} - \frac{i}{\tau}} = f^*_{-\boldsymbol{R},-1}, \tag{13}$$

with $\omega_{\boldsymbol{R}} = e\boldsymbol{E}_0 \cdot \boldsymbol{R}/\hbar$. The response at frequency ω can then be written as $j^{(1)}_a = \sigma_{ab}\mathcal{E}_{1b}$ where $a, b = x, y$ and summation over repeated indices is implied. This leads us to the main result of this work: the *dressed* optical conductivity

$$\begin{aligned}\sigma_{ab}(\omega, \boldsymbol{E}_0) = {} & \frac{ie^2}{\hbar^2 V_c} \sum_{\boldsymbol{R}} \frac{R_a R_b \varepsilon_{-\boldsymbol{R}} f^0_{\boldsymbol{R}}}{(1 - i\omega_{\boldsymbol{R}}\tau)(\omega - \omega_{\boldsymbol{R}} - \frac{i}{\tau})} \\ & - \frac{e^2}{\hbar V_c} \sum_{\boldsymbol{R}} \frac{\Omega_{-\boldsymbol{R}} f^0_{\boldsymbol{R}}}{1 - i\omega_{\boldsymbol{R}}\tau} \left[\epsilon_{ab} + \frac{e\epsilon_{ac} E_{0c} R_b/\hbar}{\omega - \omega_{\boldsymbol{R}} - \frac{i}{\tau}}\right],\end{aligned} \tag{14}$$

where ϵ_{ab} is the permutation symbol and $\sigma_{ab}(\omega, \boldsymbol{E}_0)^* = \sigma_{ab}(-\omega, \boldsymbol{E}_0)$ such that the real (imaginary) part is even (odd) in ω. As a check, we undress the conductivity by setting $E_0 = 0$. In this case, the two terms in Eq. (14) reduce to the Drude and anomalous Hall conductivity, respectively. Importantly, the dressed linear Hall response does *not* vanish when time-reversal symmetry is conserved, because it is effectively a compound nonlinear response in the fields $\boldsymbol{E}_0$ and $\boldsymbol{E}_1(t)$.

Let us now focus on the case where $\boldsymbol{E}_0$ is finite and consider the dressed longitudinal $\sigma_L = \delta_{ab}\sigma_{ab}/2$ and Hall $\sigma_H = \epsilon_{ab}\sigma_{ab}/2$ conductivities, which transform as a scalar and pseudoscalar, respectively [34]. We obtain

$$\sigma_L = \frac{ie^2}{2\hbar^2 V_c} \sum_{\boldsymbol{R}} \frac{R^2 \varepsilon_{-\boldsymbol{R}} f^0_{\boldsymbol{R}}}{(1 - i\omega_{\boldsymbol{R}}\tau)(\omega - \omega_{\boldsymbol{R}} - \frac{i}{\tau})}, \tag{15}$$

$$\sigma_H = -\frac{e^2}{\hbar V_c} \sum_{\boldsymbol{R}} \frac{\Omega_{-\boldsymbol{R}} f^0_{\boldsymbol{R}}}{1 - i\omega_{\boldsymbol{R}}\tau} \left(1 + \frac{1}{2}\frac{\omega_{\boldsymbol{R}}}{\omega - \omega_{\boldsymbol{R}} - \frac{i}{\tau}}\right), \tag{16}$$

which for $\omega_B\tau \gg 1$ simplify to

$$\sigma_L(\omega, \boldsymbol{E}_0) = -\frac{e^2}{h}\frac{\pi}{\tau V_c} \sum_{\boldsymbol{R}} \frac{R^2 \varepsilon_{-\boldsymbol{R}} f^0_{\boldsymbol{R}}}{\hbar\omega_{\boldsymbol{R}}(\omega - \omega_{\boldsymbol{R}} - \frac{i}{\tau})}, \tag{17}$$

$$\sigma_H(\omega, \boldsymbol{E}_0) = -\frac{e^2}{h}\frac{\pi}{\tau V_c} \sum_{\boldsymbol{R}} \frac{i\Omega_{-\boldsymbol{R}} f^0_{\boldsymbol{R}}}{\omega - \omega_{\boldsymbol{R}} - \frac{i}{\tau}}. \tag{18}$$

For crystals with time-reversal symmetry, the band dispersion (Berry curvature) is an even (odd) function of momentum, such that $\varepsilon_{\boldsymbol{R}}$ and $f^0_{\boldsymbol{R}}$ are real, while $\Omega_{\boldsymbol{R}}$ is imaginary. In this case, and for $\omega_B\tau \gg 1$, we see that $\mathrm{Im}\sigma_L$ and $\mathrm{Im}\sigma_H$ are given by a series of Lorentzians centered at the Bloch frequencies $\omega_{\boldsymbol{R}}$. The height of these resonances is proportional to $\varepsilon_{\boldsymbol{R}}$ and $\Omega_{\boldsymbol{R}}$, respectively, and independent of the relaxation time τ. Conversely, the real part of the dressed conductivity vanishes at resonance. Hence, σ_L is purely reactive while σ_H is purely absorptive at Bloch resonance. For linearly polarized light, the system does not dissipate, since it is essentially collisionless on the timescale set by Bloch oscillations for $\omega_B\tau \gg 1$. However, for circularly polarized light the Hall response couples dissipatively via $\mathrm{Im}\sigma_H$ since it lags in phase by a quarter cycle (see also SM [33]).

These results can thus potentially be used to map out the distribution of the Berry curvature in systems with time-reversal symmetry by measuring the resonances in the dressed optical Hall conductivity in the nonperturbative regime where $\omega_B\tau \gg 1$.

First-shell approximation.—It is instructive to first evaluate the dressed optical conductivity by only taking into account the leading-order terms in the sum over the lattice vectors. For concreteness, we consider a system with point group D_3 or C_{3v} which lacks inversion or $\mathcal{C}_{2z}$ rotation symmetry. In this case, the Berry curvature is generally nonzero even though the Chern number of the band vanishes. In the first-shell approximation, we only take into account the shortest nonzero lattice vectors such that $\varepsilon_{\boldsymbol{k}} = \varepsilon_1 \sum_{n=1}^3 \cos(\boldsymbol{k} \cdot \boldsymbol{L}_n)$ up to an additive constant and $\Omega_{\boldsymbol{k}} = \Omega_1 \sum_{n=1}^3 \sin(\boldsymbol{k} \cdot \boldsymbol{L}_n)$ where ε_1 and Ω_1 are real parameters that depend on the details of the system, and $\boldsymbol{L}_1 = L(1/2, \sqrt{3}/2)$, $\boldsymbol{L}_2 = (-L, 0)$, and $\boldsymbol{L}_3 = -(\boldsymbol{L}_1 + \boldsymbol{L}_2)$ are related by $\mathcal{C}_{3z}$ rotation symmetry [13,14].

The imaginary part of the dressed optical Hall conductivity is shown in Fig. 1(c) as a function of ω for $\theta_0 = 15°$ and different values of $\omega_B\tau$. There are three resonances in this case because the first coordination shell supports three Bloch frequencies $\omega_n = |e\boldsymbol{E}_0 \cdot \boldsymbol{L}_n/\hbar|$ which are nondegenerate for general θ_0. The height of these resonances is approximately equal due to $\mathcal{C}_{3z}$ and time-reversal symmetry and saturates to $e^2\Omega_1 f^0_1/2\hbar V_c$ in the limit $\omega_B\tau \gg 1$, where $f^0_1 = f^0_{\boldsymbol{R}=\boldsymbol{L}_n}$. Notice that the resonances are only well defined for $\omega_B\tau \gtrsim 10$. The dependence on the direction of the static field is shown in Fig. 1(d). Here, we show $\mathrm{Im}\sigma_H$ for $\omega_B\tau = 15$ as a function of ω and θ_0. As we rotate the static field, resonances move along the curves $\omega = \omega_B|\cos(\theta_0 - \theta_n)|$ with $\theta_n = \{\pi/3, \pi, -\pi/3\}$. For the special case $\theta_0 = m\pi/3$ $(m \in \mathbb{Z})$ two Bloch frequencies coincide and the peaks are doubled. On the contrary, for $\theta_0 = (2m+1)\pi/6$ the response vanishes due to $\mathcal{M}_x$ $(x \mapsto -x)$ mirror symmetry. These features can also be seen in the rose plots of Fig. 2. Here, we clearly see that the strongest resonance occurs when two lattice vectors have the same projection along the static field. Away from these directions, the resonance splits into two peaks that shift to higher and lower frequencies.

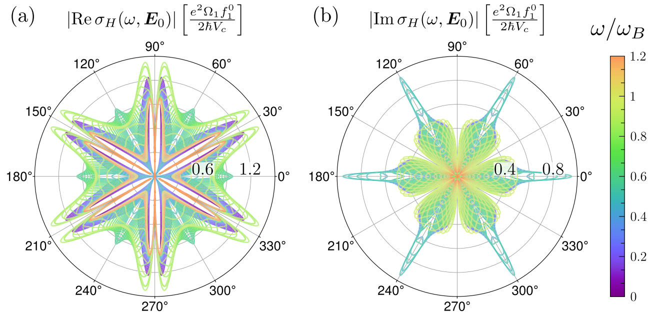

FIG. 2. Roses for the real (a) and imaginary (b) part of the dressed optical Hall conductivity $\sigma_H(\omega, \boldsymbol{E}_0)$ for the Berry curvature shown in Fig. 1(b) with $\omega_B\tau = 15$. The angle corresponds to the direction of the static electric field θ_0 and the color scale gives the frequency ω of the oscillating field.

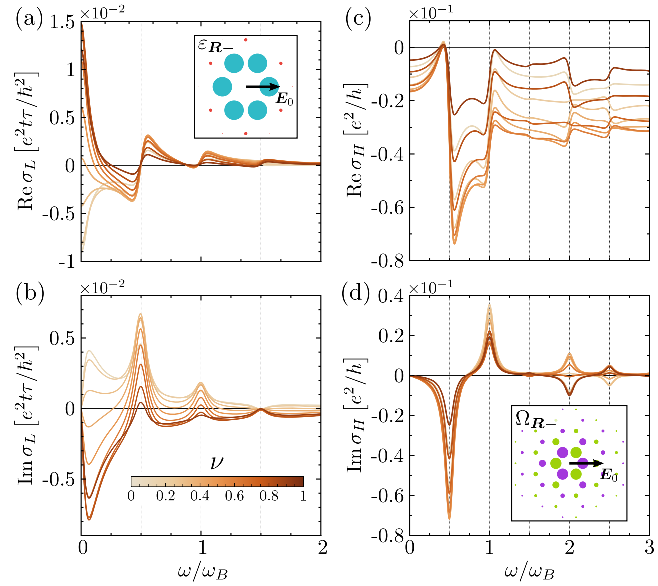

FIG. 3. Dressed optical conductivities $\sigma_L(\omega, \boldsymbol{E}_0)$ and $\sigma_H(\omega, \boldsymbol{E}_0)$ for the valence band of the two-band model with $m/t = 0.5$ where $\omega_B\tau = 15$, $\theta_0 = 0°$, and $k_BT/t = 0.004$. The color scale gives the filling $\nu \in [0.1, 0.9]$ in 0.1 increments [see inset of (b)]. (a), (b) Real and imaginary part of $\sigma_L(\omega, \boldsymbol{E}_0)$. (c), (d) Real and imaginary part of $\sigma_H(\omega, \boldsymbol{E}_0)$. Dashed vertical lines give the position of the resonances $\omega_{\boldsymbol{R}}$ and the inset in (a) and (d) shows the relative magnitude (size of dots) and phase (color) of $\varepsilon_{\boldsymbol{R}-}$ and $\Omega_{\boldsymbol{R}-}$, respectively.

Low-energy model.—Going beyond the first-shell approximation, we now consider a low-energy model defined on an effective honeycomb lattice with one orbital per site, and with nearest-neighbor hopping amplitude $t > 0$ and a sublattice-staggering potential m. The Bloch Hamiltonian is given by

$$\mathcal{H}(\boldsymbol{k}) = \boldsymbol{d}(\boldsymbol{k}) \cdot \boldsymbol{\sigma}, \tag{19}$$

$$\boldsymbol{d}(\boldsymbol{k}) = (-t\mathrm{Re}g_{\boldsymbol{k}}, -t\mathrm{Im}g_{\boldsymbol{k}}, m), \tag{20}$$

where $\boldsymbol{\sigma} = (\sigma_x, \sigma_y, \sigma_z)$ are the Pauli matrices and $g_{\boldsymbol{k}} = e^{-i\boldsymbol{k}\cdot\boldsymbol{\tau}}[1 + e^{i\boldsymbol{k}\cdot\boldsymbol{L}_1} + e^{i\boldsymbol{k}\cdot(\boldsymbol{L}_1+\boldsymbol{L}_2)}]$ with $\boldsymbol{\tau} = L\hat{y}/\sqrt{3}$ the relative separation of the two sublattices. Note that we work in periodic gauge for which the semiclassical equation given in Eq. (2) is valid [28,30]. This model has time-reversal symmetry with point group C_{3v} generated by $\mathcal{C}_{3z}$ and $\mathcal{M}_x$, and can be seen as a minimal low-energy model for moirés such as h-BN–aligned twisted bilayer graphene [35,36] or twisted double bilayer graphene [37,38], as well as other systems with the same point group, e.g., periodically buckled graphene with a C_{3v} height profile [14,39–41].

The model gives two energy bands $\varepsilon_{\boldsymbol{k}\pm} = \pm|\boldsymbol{d}(\boldsymbol{k})|$ that are separated by a gap $|2m|$ at the zone corners. Because $\mathcal{C}_{2z}$ symmetry is broken by the sublattice potential, the Berry curvature is nonzero and given by

$$\Omega_{\boldsymbol{k}\pm} = \pm\frac{mt^2V_c}{6|\boldsymbol{d}(\boldsymbol{k})|^3}\sum_{n=1}^{3}\sin(\boldsymbol{k}\cdot\boldsymbol{L}_n), \tag{21}$$

with $V_c = \sqrt{3}L^2/2$. In the limit $|m/t| \gg 1$, we have $|\boldsymbol{d}(\boldsymbol{k})| \simeq |m|$ and the first shell dominates with $\Omega_1 = \pm\mathrm{sgn}(m)V_ct^2/6m^2$. However, in general many shells contribute, as illustrated in Fig. 3 where we show $\sigma_L(\omega, \boldsymbol{E}_0)$ in panels (a) and (b), and $\sigma_H(\omega, \boldsymbol{E}_0)$ in panels (c) and (d) for $m/t = 0.5$ and different fillings ν of the valence band. Here, the static field lies along the x direction and $k_BT/t \ll 1$. Note σ_L decays faster with frequency than σ_H because the first shell of the dispersion is dominant [see inset of Fig. 3(a)] and because of the additional factor of $1/\omega$ in Eq. (17). The filling ν enters only through the Fourier components of the Fermi function $f^0_{\boldsymbol{R}}$ which modulate the height of the peaks in the imaginary part of the conductivities and can change sign as a function of ν, see Fig. 3(d).

In conclusion, we developed a band-projected semiclassical theory for the optical response of an artificial crystal, such as a moiré material, that is dressed by a uniform static field. When the static field is sufficiently strong, achieved for field strengths of order 10 kV/cm for a lattice constant of order 10 nm, the dressed system becomes resonant at the Bloch frequencies which are in the 10 THz regime. We quantified this effect by defining a dressed optical conductivity whose imaginary part displays resonant peaks, while the real part vanishes at resonance. In particular, the height of the resonances in the optical Hall conductivity probe the lattice Fourier components of the Berry curvature and are independent of the relaxation time. One thus obtains an intrinsic probe of the quantum geometry of the band by resonantly coupling light to Bloch oscillations. The dressed optical conductivity can, for example, be obtained from terahertz Faraday rotation and ellipticity spectroscopy measurements [42,43]. In contrast to probes of the Berry curvature multipoles, such at the rectified second-order response involving the Berry curvature dipole [4], our proposal works at linear order in the optical response, and works best for a smooth Berry curvature dominated by the first coordination shell whose lowest multipoles are zero or small. Moreover, by changing the in-plane direction of the static field, one can tune contributions from different lattice vectors. This work thus provides a novel route to probe the Berry curvature in time-reversal symmetric moiré and other artificial crystals which have a large real-space periodicity.

We thank V. T. Phong for discussions. This research was funded in whole, or in part, by the Luxembourg National Research Fund (FNR) (Project No. 16515716). C. D. B. and E. J. M. are supported by the Department of Energy under Grant No. DE-FG02-84ER45118.

*Corresponding author: cdebeule@sas.upenn.edu

[1] T. Morimoto and N. Nagaosa, Topological nature of nonlinear optical effects in solids, Sci. Adv. **2**, e1501524 (2016).
[2] L. Wu, S. Patankar, T. Morimoto, N. L. Nair, E. Thewalt, A. Little, J. G. Analytis, J. E. Moore, and J. Orenstein, Giant anisotropic nonlinear optical response in transition metal monopnictide Weyl semimetals, Nat. Phys. **13**, 350 (2017).
[3] J. Ahn, G.-Y. Guo, N. Nagaosa, and A. Vishwanath, Riemannian geometry of resonant optical responses, Nat. Phys. **18**, 290 (2022).
[4] I. Sodemann and L. Fu, Quantum nonlinear Hall effect induced by Berry curvature dipole in time-reversal invariant materials, Phys. Rev. Lett. **115**, 216806 (2015).
[5] C.-P. Zhang, X.-J. Gao, Y.-M. Xie, H. C. Po, and K. T. Law, Higher-order nonlinear anomalous Hall effects induced by Berry curvature multipoles, Phys. Rev. B **107**, 115142 (2023).
[6] E. Y. Andrei and A. H. MacDonald, Graphene bilayers with a twist, Nat. Mater. **19**, 1265 (2020).
[7] E. Y. Andrei, D. K. Efetov, P. Jarillo-Herrero, A. H. MacDonald, K. F. Mak, T. Senthil, E. Tutuc, A. Yazdani, and A. F. Young, The marvels of moiré materials, Nat. Rev. Mater. **6**, 201 (2021).
[8] K. F. Mak and J. Shan, Semiconductor moiré materials, Nat. Nanotechnol. **17**, 686 (2022).
[9] R. Tsu, *Superlattice to Nanoelectronics* (Elsevier Science, Amsterdam, 2005).
[10] C. Forsythe, X. Zhou, K. Watanabe, T. Taniguchi, A. Pasupathy, P. Moon, M. Koshino, P. Kim, and C. R. Dean, Band structure engineering of 2D materials using patterned dielectric superlattices, Nat. Nanotechnol. **13**, 566 (2018).
[11] J. Mao, S. P. Milovanović, M. Anđelković, X. Lai, Y. Cao, K. Watanabe, T. Taniguchi, L. Covaci, F. M. Peeters, A. K. Geim, Y. Jiang, and E. Y. Andrei, Evidence of flat bands and correlated states in buckled graphene superlattices, Nature (London) **584**, 215 (2020).
[12] A. Fahimniya, Z. Dong, E. I. Kiselev, and L. Levitov, Synchronizing Bloch-oscillating free carriers in moiré flat bands, Phys. Rev. Lett. **126**, 256803 (2021).
[13] V. T. Phong and E. J. Mele, Quantum geometric oscillations in two-dimensional flat-band solids, Phys. Rev. Lett. **130**, 266601 (2023).
[14] C. D. Beule, V. T. Phong, and E. J. Mele, Roses in the nonperturbative current response of artificial crystals, Proc. Natl. Acad. Sci. U.S.A. **120**, 2306384120 (2023).
[15] P. A. Pantaleón, T. Low, and F. Guinea, Tunable large Berry dipole in strained twisted bilayer graphene, Phys. Rev. B **103**, 205403 (2021).
[16] Z. He and H. Weng, Giant nonlinear Hall effect in twisted bilayer WTe_2, npj Quantum Mater. **6**, 101 (2021).
[17] S. Sinha, P. C. Adak, A. Chakraborty, K. Das, K. Debnath, L. D. V. Sangani, K. Watanabe, T. Taniguchi, U. V. Waghmare, A. Agarwal, and M. M. Deshmukh, Berry curvature dipole senses topological transition in a moiré superlattice, Nat. Phys. **18**, 765 (2022).
[18] A. Chakraborty, K. Das, S. Sinha, P. C. Adak, M. M. Deshmukh, and A. Agarwal, Nonlinear anomalous Hall effects probe topological phase-transitions in twisted double bilayer graphene, 2D Mater. **9**, 045020 (2022).
[19] C.-P. Zhang, J. Xiao, B. T. Zhou, J.-X. Hu, Y.-M. Xie, B. Yan, and K. T. Law, Giant nonlinear Hall effect in strained twisted bilayer graphene, Phys. Rev. B **106**, L041111 (2022).
[20] P. A. Pantaleón, V. o. T. Phong, G. G. Naumis, and F. Guinea, Interaction-enhanced topological Hall effects in strained twisted bilayer graphene, Phys. Rev. B **106**, L161101 (2022).
[21] J. Duan, Y. Jian, Y. Gao, H. Peng, J. Zhong, Q. Feng, J. Mao, and Y. Yao, Giant second-order nonlinear Hall effect in twisted bilayer graphene, Phys. Rev. Lett. **129**, 186801 (2022).
[22] J. Zhong, J. Duan, S. Zhang, H. Peng, Q. Feng, Y. Hu, Q. Wang, J. Mao, J. Liu, and Y. Yao, Effective manipulation and realization of a colossal nonlinear Hall effect in an electric-field tunable moiré system, arXiv:2301.12117.
[23] F. Bloch, Über die quantenmechanik der elektronen in kristallgittern, Z. Phys. **52**, 555 (1929).
[24] K. Leo, P. H. Bolivar, F. Brüggemann, R. Schwedler, and K. Köhler, Observation of Bloch oscillations in a semiconductor superlattice, Solid State Commun. **84**, 943 (1992).
[25] T. T. Luu and H. J. Wörner, Measurement of the Berry curvature of solids using high-harmonic spectroscopy, Nat. Commun. **9**, 916 (2018).
[26] M. Schüler, U. D. Giovannini, H. Hübener, A. Rubio, M. A. Sentef, and P. Werner, Local Berry curvature signatures in dichroic angle-resolved photoelectron spectroscopy from two-dimensional materials, Sci. Adv. **6**, eaay2730 (2020).
[27] M.-C. Chang and Q. Niu, Berry phase, hyperorbits, and the Hofstadter spectrum, Phys. Rev. Lett. **75**, 1348 (1995).
[28] G. Sundaram and Q. Niu, Wave-packet dynamics in slowly perturbed crystals: Gradient corrections and Berry-phase effects, Phys. Rev. B **59**, 14915 (1999).
[29] To construct a wave packet $|W(t)\rangle = \int_{\boldsymbol{k}} c_{\boldsymbol{k}}(t)|\Psi_{\boldsymbol{k}}\rangle$, the Bloch states $|\Psi_{\boldsymbol{k}}\rangle = e^{i\boldsymbol{k}\cdot\hat{\boldsymbol{r}}}|u_{\boldsymbol{k}}\rangle$ should be smooth on the BZ torus, i.e., $|\Psi_{\boldsymbol{k}+\boldsymbol{G}}\rangle = |\Psi_{\boldsymbol{k}}\rangle$ with $\boldsymbol{G}$ a reciprocal lattice vector. This is periodic gauge [30] and yields $|u_{\boldsymbol{k}+\boldsymbol{G}}\rangle = e^{-i\boldsymbol{G}\cdot\hat{\boldsymbol{r}}}|u_{\boldsymbol{k}}\rangle$, in contrast to $|\tilde{u}_{\boldsymbol{k}+\boldsymbol{G}}\rangle = |\tilde{u}_{\boldsymbol{k}}\rangle$ for which the Bloch Hamiltonian is periodic (Bloch form). The Berry curvature is generally different in both gauges.

[30] D. Vanderbilt, *Berry Phases in Electronic Structure Theory* (Cambridge University Press, Cambridge, 2018).
[31] N. W. Ashcroft and N. D. Mermin, *Solid State Physics* (Saunders College Publishing, Philadelphia, 1976).
[32] S. A. Mikhailov, Nonperturbative quasiclassical theory of the nonlinear electrodynamic response of graphene, Phys. Rev. B **95**, 085432 (2017).
[33] See Supplemental Material at http://link.aps.org/supplemental/10.1103/PhysRevLett.131.196603 for a detailed calculation of the occupation function and the dressed optical conductivity.
[34] Note that one also has to transform $\boldsymbol{E}_0$ such that σ_H is nonzero even in the presence of mirror symmetry.
[35] Y.-H. Zhang, D. Mao, and T. Senthil, Twisted bilayer graphene aligned with hexagonal boron nitride: Anomalous Hall effect and a lattice model, Phys. Rev. Res. **1**, 033126 (2019).
[36] C. Lewandowski and L. Levitov, Intrinsically undamped plasmon modes in narrow electron bands, Proc. Natl. Acad. Sci. U.S.A. **116**, 20869 (2019).
[37] M. Koshino, Band structure and topological properties of twisted double bilayer graphene, Phys. Rev. B **99**, 235406 (2019).
[38] N. R. Chebrolu, B. L. Chittari, and J. Jung, Flat bands in twisted double bilayer graphene, Phys. Rev. B **99**, 235417 (2019).
[39] S. P. Milovanović, M. Aneđelković, L. Covaci, and F. M. Peeters, Band flattening in buckled monolayer graphene, Phys. Rev. B **102**, 245427 (2020).
[40] V. T. Phong and E. J. Mele, Boundary modes from periodic magnetic and pseudomagnetic fields in graphene, Phys. Rev. Lett. **128**, 176406 (2022).
[41] Q. Gao, J. Dong, P. Ledwith, D. Parker, and E. Khalaf, Untwisting moiré physics: Almost ideal bands and fractional Chern insulators in periodically strained monolayer graphene, Phys. Rev. Lett. **131**, 096401 (2023).
[42] S. Spielman, B. Parks, J. Orenstein, D. T. Nemeth, F. Ludwig, J. Clarke, P. Merchant, and D. J. Lew, Observation of the quasiparticle Hall effect in superconducting $YBa_2Cu_3O_{7-\delta}$, Phys. Rev. Lett. **73**, 1537 (1994).
[43] R. Shimano, Y. Ikebe, K. S. Takahashi, M. Kawasaki, N. Nagaosa, and Y. Tokura, Terahertz Faraday rotation induced by an anomalous Hall effect in the itinerant ferromagnet $SrRuO_3$, Europhys. Lett. **95**, 17002 (2011).